STED-FLCS

An Advanced Tool to Reveal Spatiotemporal Heterogeneity of Molecular Membrane Dynamics

Vicidomini, Giuseppe; Ta, Haisen; Honigmann, Alf; Mueller, Veronika; Clausen, Mathias P.; Waithe, Dominic; Galiani, Silvia; Sezgin, Erdinc; Diaspro, Alberto; Hell, Stefan W.; Eggeling, Christian

Published in:
Nano Letters

DOI:
10.1021/acs.nanolett.5b02001

Publication date:
2015

Document version
Publisher's PDF, also known as Version of record

NANO LETTERS

Letter

pubs.acs.org/NanoLett

STED-FLCS: An Advanced Tool to Reveal Spatiotemporal Heterogeneity of Molecular Membrane Dynamics

Giuseppe Vicidomini,*[,†,‡] Haisen Ta,[‡] Alf Honigmann,[‡,§] Veronika Mueller,[‡] Mathias P. Clausen,[∥,⊥] Dominic Waithe,[∥] Silvia Galiani,[∥] Erdinc Sezgin,[∥] Alberto Diaspro,[†] Stefan W. Hell,[‡] and Christian Eggeling*[,∥,‡]

[†]Nanoscopy, Nanophysics, Instituto Italiano di Tecnologia, Via Morego 30, 16163 Genoa, Italy

[‡]Department of NanoBiophotonics, Max Planck Institute for Biophysical Chemistry, Am Fassberg 11, 37077 Goettingen, Germany

[§]Max Planck Institute for Molecular Cell Biology and Genetics, Pfotenhauerstr. 108, 01309 Dresden, Germany

[∥]MRC Human Immunology Unit and Wolfson Imaging Centre Oxford, Weatherall Institute of Molecular Medicine, Radcliffe Department of Molecular Medicine, University of Oxford, OX3 9DS Oxford, United Kingdom

[⊥]MEMPHYS−Center for Biomembrane Physics, University of Southern Denmark, Campusvej 55, Odense MDK-5230, Denmark

Supporting Information

ABSTRACT: Heterogeneous diffusion dynamics of molecules play an important role in many cellular signaling events, such as of lipids in plasma membrane bioactivity. However, these dynamics can often only be visualized by single-molecule and super-resolution optical microscopy techniques. Using fluorescence lifetime correlation spectroscopy (FLCS, an extension of fluorescence correlation spectroscopy, FCS) on a super-resolution stimulated emission depletion (STED) microscope, we here extend previous observations of nanoscale lipid dynamics in the plasma membrane of living mammalian cells. STED-FLCS allows an improved determination of spatiotemporal heterogeneity in molecular diffusion and interaction dynamics via a novel gated detection scheme, as demonstrated by a comparison between STED-FLCS and previous conventional STED-FCS recordings on fluorescent phosphoglycerolipid and sphingolipid analogues in the plasma membrane of live mammalian cells. The STED-FLCS data indicate that biophysical and biochemical parameters such as the affinity for molecular complexes strongly change over space and time within a few seconds. Drug treatment for cholesterol depletion or actin cytoskeleton depolymerization not only results in the already previously observed decreased affinity for molecular interactions but also in a slight reduction of the spatiotemporal heterogeneity. STED-FLCS specifically demonstrates a significant improvement over previous gated STED-FCS experiments and with its improved spatial and temporal resolution is a novel tool for investigating how heterogeneities of the cellular plasma membrane may regulate biofunctionality.

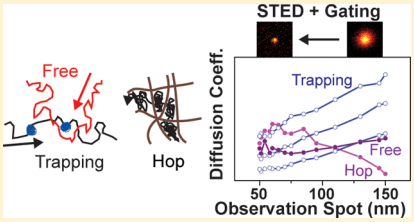

KEYWORDS: *Super-resolved microscopy, stimulated-emission-depletion microscopy, time-resolved, fluorescence-correlation spectroscopy, time-correlated single-photon counting*

The role of the cellular plasma membrane is central in many biological processes. It is well acknowledged that the plasma membrane is not just a simple fluidic system, but it is rather a highly heterogeneous environment constituting a plethora of different lipids, proteins, and sugars, with links to the underlying actin cytoskeleton and the extracellular matrix. Important cellular functions are often triggered by specific interactions between these entities.[1−3] Such interactions usually result in highly heterogeneous diffusion patterns of the involved molecules[4,5] (Figure 1a). For example, molecules will not diffuse freely but are transiently trapped when interacting with immobilized or slow moving entities. Further, compartmentalization of the membrane by the underlying actin cytoskeleton can result in a hindered, e.g., hop-like, diffusion.

A widespread tool for investigating molecular diffusion dynamics is fluorescence correlation spectroscopy (FCS), which determines average molecular diffusion coefficients D from thousands of molecular transits through the microscope's observation spot.[6,7] With measurement times of only a few seconds, and by placing or scanning the spot over distinct points in space, FCS may deliver information on heterogeneity in diffusion over space and time.[8,9] Revealing heterogeneous diffusion modes requires probing diffusion coefficients D at different spatial scales, i.e., for different observation spot diameters d[5,10] (Figure 1b). Unfortunately, due to the limited spatial resolution of conventional far-field microscopy, nanoscopic details of such heterogeneity are usually only indirectly inferable in such spot-variation FCS experiments, by extrapolating to relevant sub-100 nm spatial scales.

A remedy to this limitation is the use of FCS on a super-resolution stimulated emission depletion (STED) micro-

Received: May 21, 2015
Revised: July 29, 2015
Published: August 3, 2015

DOI: 10.1021/acs.nanolett.5b02001
Nano Lett. 2015, 15, 5912−5918

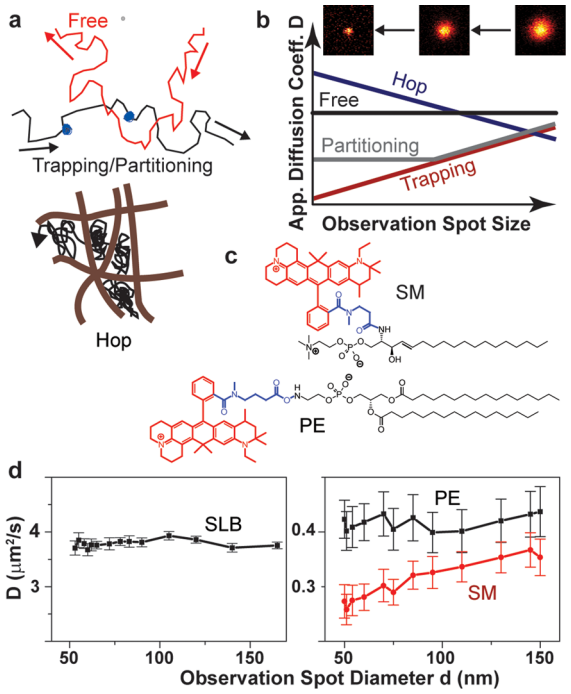

Figure 1. Diffusion modes and impact on STED-FCS measurements. (a) Sketch of representative molecular tracks for different diffusion modes, such as free diffusion (red, upper), trapping diffusion or transient partitioning into domains of higher molecular order (blue, upper, with dots marking the points of transient stops in diffusion), and hop diffusion (black, lower) due to compartmentalization of the membrane by the underlying actin meshwork (brown). (b) Schematic dependency of the apparent diffusion coefficient D on the diameter d of the observation spot, as expected for the different diffusion modes and as for example determined by STED-FCS. Insets: Exemplary observation spots of decreasing size (arrows) as formed by scanning over single emitters for increasing STED intensities. (c) Molecular structures of the fluorescent lipid analogues PE (phosphoethanolamine, acyl chain length C15, saturated, label at headgroup) and SM (sphingomyelin, C13, saturated, labeling via acyl-chain replacement) labeled with the organic dye Atto647N (red) as used in this study. (d) Dependency $D(d)$ measured by single-point STED-FCS for PE in a supported lipid bilayer (SLB, DOPC MICA-supported lipid bilayer, left) and for PE and SM in the plasma membrane of live PtK2 cells (right, PE, black; SM, red), exemplifying free diffusion of PE in both cases, trapping diffusion for SM in cells, and an increased heterogeneity for diffusion in cells (error bars as s.d.m. from 20 measurements).

scope.[11] STED microscopy delivers spatial resolution of <50 nm in living cells and allows a straightforward tuning of the observation spot by the intensity of the added STED laser beam, i.e., a straightforward determination of the $D(d)$ dependency down to the relevant scale.[12,13] Using STED-FCS, we have previously shown that this $D(d)$ dependency varies for the diffusion characteristics of fluorescent lipid analogues of phosphoethanolamine (PE) and sphingomyelin (SM) (Figure 1c) in the plasma membrane of live mammalian PtK2 cells, revealing transient trapping for the SM analogue (once again experimentally verified in Figure 1d). Close inspection of the FCS data at small d and for different lipid analogues revealed that, at least for the cell types investigated:[12−14] (i) trapping was due to lipid-specific transient interactions with other membrane entities such as proteins on time-scales of 1−10 ms; (ii) that the lipids hardly moved during trapping (i.e., the binding partner is relatively slow-moving or even immobilized); (iii) that trapping was locally confined in spots of <80 nm in size that were transient in the time scale of 1−10 s; and (iv) that these interactions were independent of the lipid's preference for liquid-ordered or -disordered environments in model membranes (often referred to as "rafts"). Furthermore, with previous control experiments using different dye labels and label positions as well as different experimental conditions,[12−15] we ensured a nondetectable (at least by STED-FCS) influence by the dye label on the lipid dynamics, by photobleaching, heating, or other (nonlinear) laser-driven effects, and the accurate integration of the lipid analogues into the membrane. Moreover, as expected[16] diffusion of both the Atto647N-labeled PE and SM was free in a fluid model membrane such as (100% DOPC) supported lipid bilayers (SLBs) on plasma-cleaned glass, as here experimentally verified in Figures 1d and S1.

In the previous STED-FCS experiments, the recording of the $D(d)$ dependency took at least minutes since it required the recording of at least 5−15 s-long FCS data for various intensities of the STED laser, with an unavoidable displacement of the observation (i.e., laser) spot in-between measurements. As a consequence, the STED-FCS experiments averaged over temporal and spatial heterogeneity. Notably, the standard deviations of the averaged values determined for D in live-cell membranes were much larger than those recorded for the fluorescent lipid analogues diffusing in the fluid SLB (Figure 1d), revealing a hidden heterogeneity in the plasma membrane data. To better highlight heterogeneity in diffusion modes, we urged for a measurement mode that can access the $D(d)$ dependency within one FCS recording, i.e., within 5−15 s only.

Most STED-FCS experiments so far employed pulsed laser light for both excitation and stimulated emission action. In this configuration, the only way to tune the observation spot is by varying the intensity of the STED laser, which is unfortunately not straightforwardly realizable within a single FCS recording. However, we have previously shown that in an experimental arrangement that uses pulsed excitation, continuous-wave (CW) STED laser beams and time-gated detection, the observation spot size d can also be tuned by the position of the time gate (gated STED, gSTED).[17,18] This is because in this arrangement, the (cumulative) probability for stimulated emission increases over time after the excitation laser pulse, and thus, fluorescence photons detected after different time-delays, i.e., at different time-gates starting from time T_g with respect to the excitation laser pulse, originate from increasingly decreased central areas of the observation spot[18,19] (Figure S2). As a consequence, FCS data can be generated for different observation spot sizes d and thus the $D(d)$ dependencies constituted out of a single measurement (not requiring recordings at multiple STED intensities as before). Specifically, by setting different time gates T_g and calculating data from photons arriving only at times > T_g, different correlation data are acquired out of a single photon stream recorded by time-correlated single-photon counting (TCSPC) for one STED laser beam intensity (Figure 2a).[18] However, the gSTED-FCS analysis in its current state is still limited. For small time delays T_g, the gSTED-FCS approach averages over a large time period of STED laser beam action, resulting already in rather reduced spot sizes d. As a consequence, the range of diameters accessed by gated STED-FCS from a measurement at a single STED laser beam intensity is rather low, e.g., 50 nm < d < 110 nm, as determined both theoretically (Figure S3d) and experimentally (Figure 2b, gated STED-FCS analysis of free diffusion of PE in

DOI: 10.1021/acs.nanolett.5b02001
Nano Lett. 2015, 15, 5912−5918

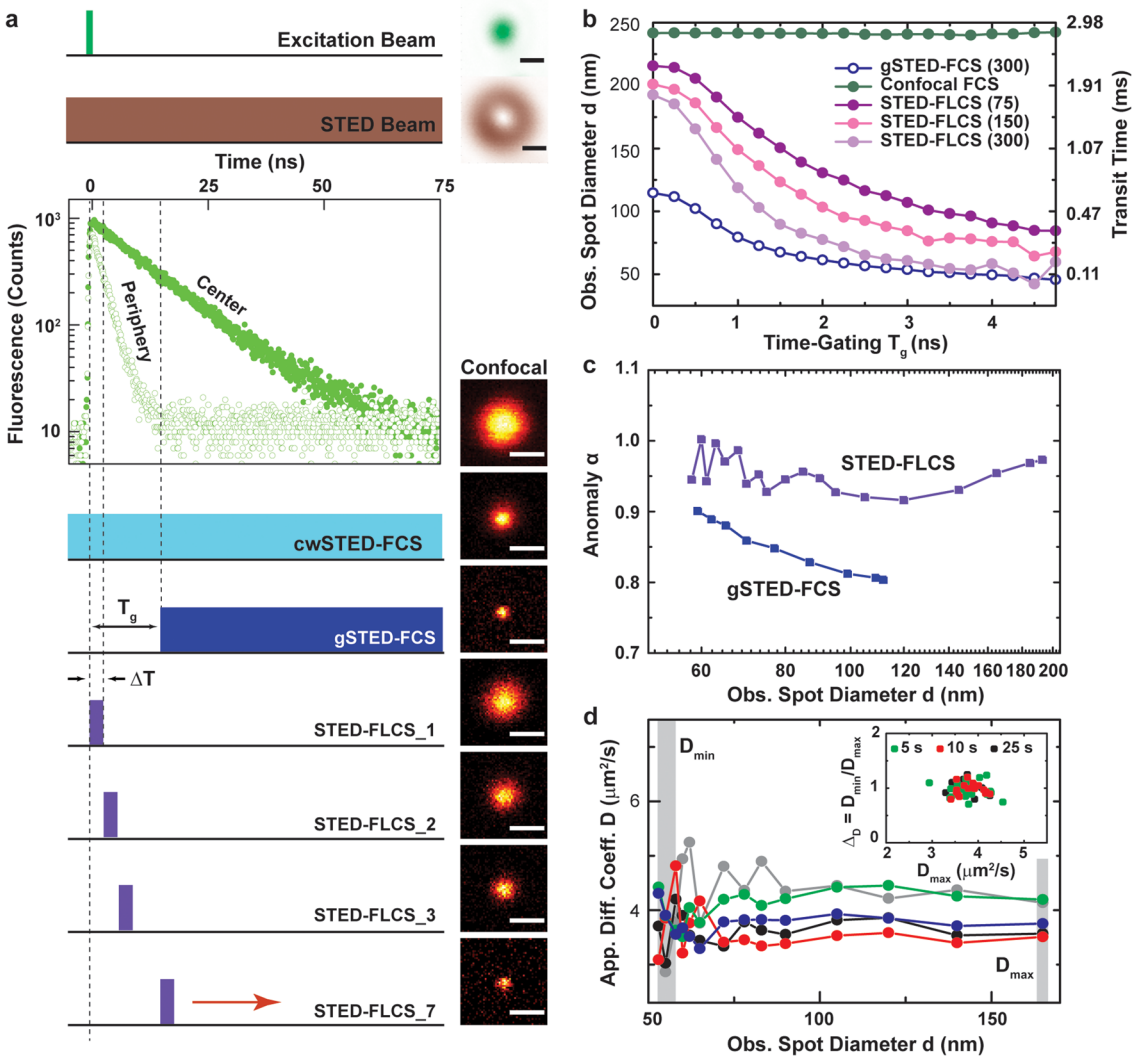

Figure 2. Principle of STED-FLCS. (a) Time t courses (left panels) of the excitation laser (green, upper, sketched), the STED laser (brown, below, sketched), decay of fluorescence emission (middle, experimental data from single emitter) at the focal center (green) and periphery (hollow green), and detection windows (lower panels) for cwSTED-FCS (light blue), gSTED-FCS (dark blue with time gate T_g), and STED-FLCS (violet) with detection window ΔT and for increasing time gate T_g (red arrow). The right panels show experimental images of the focal intensity distribution of the excitation (upper, green) and STED (second upper, brown) lasers, as well as the fluorescence images of a single emitter as obtained for the different gating conditions, as labeled or indicated in the left panels. Scale bars 200 nm. (b) Experimentally determined dependency of the observation spot diameter d (full width at half-maximum, fwhm) on the time gate T_g for the different STED-FCS modes as indicated in the legend, and for different STED laser powers P_{STED} in the case of STED-FLCS, as indicated in brackets in mW (P_{STED}(gSTED-FCS) = 300 mW). The dynamic range in d is highest for STED-FLCS. The diameter d was determined from FCS analysis of free diffusion of the PE analogue in the SLB. (c) Dependency of anomaly α on d for the gSTED-FCS and STED-FLCS data of free diffusion of PE in the SLB (P_{STED} = 300 mW). An apparent anomaly appears in the case of gSTED-FCS, especially for small T_g, i.e, . larger d; an artifact that is avoided in the STED-FLCS recordings. (d) Representative dependencies of the apparent diffusion coefficient D on d for single 10 s STED-FLCS recordings of PE diffusion in SLBs, allowing the determination of D_{max} and D_{min} for large and small diameters, respectively (gray bars). Inset: Scatter of value pairs (D_{max}, $\Delta_D = D_{min}/D_{max}$) for 20 STED-FLCS recordings of different measurement times (green, 5 s; red, 10 s; black, 25 s), indicating low heterogeneity of diffusion with a free Brownian characteristics (center at Δ_D = 1 and D_0 = 3.8 μm^2/s).

the fluid SLB). Consequently, a full $D(d)$ dependency (from confocal >150 to 50 nm diameters) would require the recording at additional, lower STED intensities, again limiting the time resolution.

The basics of gSTED-FCS are similar to that of fluorescence-lifetime-correlation spectroscopy (FLCS), where also different FCS data is generated from the same TCSPC photon stream. In FLCS, the photons are weighted differently as to separate FCS data between labels of different fluorescence lifetime.[20,21] Starting from that idea, we here introduce STED-FLCS as an improved version of gSTED-FCS. In STED-FLCS, correlation data is separated for different observation spot sizes d by choosing photons from time gating intervals ΔT centered at different T_g (instead of from the whole time span > T_g as for gSTED-FCS) (Figure 2a). By choosing intervals ΔT instead of whole time spans, we both theoretically (Figures S2c and S3a) and experimentally (Figure 2b) showed a continuous reduction of the diameter d of the observation spot from close to diffraction-limited 240 nm down to in this case approximately 50 nm. In addition, the spatial profile of the fluorescence emission in the observation spot of the STED-FLCS data was well described by a Gaussian, while this was less the case for

DOI: 10.1021/acs.nanolett.5b02001
Nano Lett. 2015, 15, 5912−5918

gSTED-FCS (Figure S3b). Since the gSTED-FCS data, especially for small T_g, results from averaging over a large time period of STED laser beam action, the profile of the fluorescence emission in the observation spot is more Gaussian−Lorentzian.[22] gSTED-FCS data thus revealed a more stretched decay (compared to conventional FCS data resulting from free diffusion through a Gaussian-shaped observation spot), and in our case we had to introduce an anomaly $\alpha < 1$ to accurately fit the experimental gSTED-FCS data (PE diffusing freely in the fluid SLB) using conventional FCS data analysis (Figure 2c). Unfortunately, values of $\alpha < 1$ usually indicate anomalous or hindered diffusion. Thus, the accurate fitting of gated STED-FCS data would have required more complex fitting routines.[23,24] Yet, we received $\alpha \approx 1$ from the conventional FCS analysis of the STED-FLCS data instituted from the same data set (Figure 2c).

To highlight the advantages of the STED-FLCS analysis, we anticipated a direct comparison to the previous STED-FCS studies, thus using again the example of the membrane diffusion dynamics of the PE and SM analogues. Figure 2d shows representative $D(d)$ dependencies from the analysis of subsequent 5−25 s long STED-FLCS measurements of the diffusion of the PE lipid in the fluid SLB. As expected, the $D(d)$ dependencies were constant, indicating free diffusion. Also, the FCS data revealed a sufficient quality (Figure S4), and consequently the variation in parameters was very low, even for measurement times as low as 5 s. Each STED-FLCS recording let us determine two important parameters at once, the apparent diffusion coefficient D_{max} of the confocal recordings, roughly outlining the overall macroscopic mobility, and the ratio $\Delta_D = D_{min}/D_{max}$ of the apparent diffusion coefficients determined for the smallest observation spots (D_{min}) and the largest observation spot (D_{max}). This ratio is $\Delta_D = 1$ for free diffusion, <1 for heterogeneous diffusion due to, for example, transient trapping, and >1 for hop diffusion[13,14,25] (compare Figure 1b,d). For both parameters and for measurement times of 5−25 s, we observed a low scatter in values around average values of $D_{max} = 3.8\ \mu m^2/s$ and $\Delta_D = 1$, as well as expressing the negligible change in $D(d)$ and thus diffusion mode in the time regime of seconds (inset Figure 2d, for SM see Figure S1b). The observation of variation of diffusion modes on the second time scale was impossible before since D_{max} and D_{min} had to be accessed from separate measurements, i.e., with decreased time resolution.

The range of diameters d accessed for different time delays T_g within a single STED-FLCS measurement varied with the STED intensity as well as with the width ΔT of the detection windows. As shown experimentally and theoretically in Figures 2b and S5a, respectively, the smallest observation spots for determining D_{min} were created with larger STED intensities, but this also came along with a reduction of the observation spot determining D_{max}, i.e., the whole range of diameters accessed (max to min) was shifted to smaller values. While the choice of ΔT did not change the size of the smallest observation spots reached for large T_g, we more closely approached the diffraction-limited observation spot for small T_g with narrower time windows, i.e., smaller ΔT (Figure S5c). As pointed out before (Figure 2b), this results from the fact that, especially for small T_g, large ΔT entail averaging over a larger time periods of STED laser beam action. Consequently, the largest range of diameters d (max to min) within a single STED-FLCS measurement is in principle realized with small ΔT. However, smaller ΔT impose decreased number of detected photon and thus decreased signal-to-noise ratios; the signal-to-noise ratio in any case decreases with increasing T_g[18,19] (Figure S5c). Therefore, one has to balance the range of accessible d-values against signal-to-noise ratios. In our case, when using Atto647N-labeled lipids and powers P_{STED} = 300 mW of the STED light at 770 nm we achieved sufficient signal-to-noise in the FCS data for ΔT = 1.5 ns and 10 s recordings (Figure S4).

We next moved to the investigation of the diffusion characteristics of the fluorescent lipid analogues in the plasma membrane of living cells.[12−14] Using STED-FLCS with parameters as defined in the previous paragraph, various $D(d)$ dependencies were determined from 10 s recordings of the Atto647N-labeled PE and SM lipids diffusing in the plasma membrane of living Ptk2 cells at different times and places (Figures 3a and S6a). Compared to the model membrane data (Figure 2d), the $D(d)$ dependency varied strongly in time and

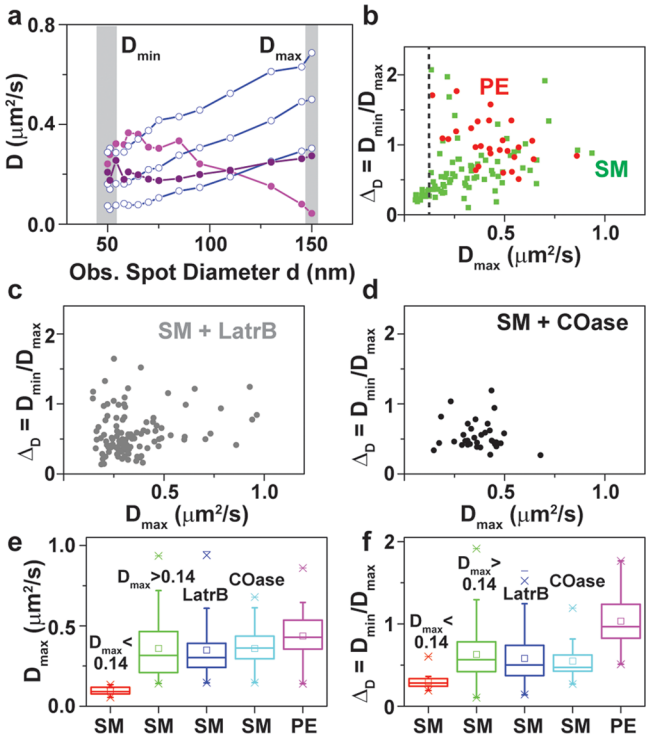

Figure 3. STED-FLCS measurements of lipid diffusion in the plasma membrane of live PtK2 cells. (a) Dependencies $D(d)$ for representative 10 s measurements of SM with the parameters D_{max} and D_{min} marked by gray bars. A large heterogeneity in diffusion modes becomes obvious (purple, free; blue, trapping; magenta, hopping). (b−d) Scatter of value pairs (D_{max} long-range apparent diffusion constant, $\Delta_D = D_{min}/D_{max}$ diffusion mode) for STED-FLCS recordings of (b) PE (red, N = 28) and SM (green, N = 84, the dotted vertical line indicates the arbitrary threshold for events of strong trapping $D_{max} < 0.14$), (c) SM following LatrB treatment for actin depolymerization (N = 109), and (d) SM following COase treatment for cholesterol depletion (N = 56). Diffusion of PE is mainly free ($\Delta_D \approx 1$), while most of the SM measurements indicate trapping ($\Delta_D \ll 1$), which is much less upon treatment with COase or LatrB. In all cases, diffusion is very heterogeneous as indicated by the strong scatter in values. (e,f) Boxplots of values of D_{max} (e) and Δ_D (f) determined from the respective data of b−d as labeled, indicating average values and standard deviations. For SM we differentiated between strong ($D_{max} < 0.14$) and weaker ($D_{max} > 0.14$) trapping events. Heterogeneity in membrane diffusion (especially in Δ_D) is slightly reduced after COase treatment.

DOI: 10.1021/acs.nanolett.5b02001
Nano Lett. 2015, 15, 5912−5918

space, with changing values in both D_{max} and Δ_D (compare also Figure S7, depicting specifically changes in D_{max} and Δ_D over time). However, averaging over a multiple of these data again revealed a $D(d)$ characteristic as in Figure 1d, with the same large standard deviations. The heterogeneity in space and time of plasma membrane lipid diffusion is further highlighted in Figure 3b, where the scatter in value pairs (D_{max}, Δ_D) is depicted for the STED-FLCS recordings of PE and SM. Both fluorescent lipid analogues not only showed vast changes in diffusion modes, mainly between free ($\Delta_D \approx 1$) to trapping ($\Delta_D \ll 1$) diffusion, but also strong changes in overall macroscopic mobility D_{max} over space and time. While the values scattered around D_{max} = 0.4 $\mu m^2/s$ and Δ_D = 1 for PE, confirming close to free diffusion, in the case of SM these parameters ranged from values similar to PE down to values as low as D_{max} < 0.1 $\mu m^2/s$ and Δ_D < 0.14, indicating trapping diffusion, i.e., interaction with less mobile membrane entities at these points in space and time. For SM, values of D_{max} and Δ_D correlated in a positive way (compare also Figure S6). This is to be expected since trapping also leads to a macroscopic slow-down.[12] Especially incidences of more pronounced free diffusion (Δ_D around 1) showed large variations in overall macroscopic mobility D_{max}, indicating, for example, variations in membrane viscosity, fluidity or molecular crowding. Therefore, distinct interaction sites and spots of different mobility changed strongly over space and time. Since values of D_{max} and Δ_D were distinct even for the STED-FLCS recordings of 10 s, the different conditions (trapping, free diffusion, or certain overall mobility) had to be stable for at least a few seconds; otherwise, they would not have dominated the respective 10 s long single recordings. These findings are in accordance with previous STED-FCS recordings using fast beam-scanning, revealing for SM several distinct interactions sites that were stable for several seconds up to 10 s.[14] However, those scanning STED-FCS recordings could not determine D_{max} and Δ_D out of one recording (but rather either only D_{max} or D_{STED}). Therefore, while scanning STED-FCS highlighted changes in space at a distinct time-point in either D_{max} or D_{min}, our current STED-FLCS recordings directly revealed changes in D_{max}, D_{min} and most importantly Δ_D over time (Figure S7). In contrast, heterogeneity in space was only approached by comparing value pairs (D_{max}, Δ_D) taken at different spots and different cells at different time points (Figure 3).

Our STED-FLCS data also observed some incidences of hop diffusion ($\Delta_D \gg 1$). In this mode, diffusion of molecules is hindered by compartments.[4,10,25,26] While molecules diffuse freely within these compartments, diffusion from one compartment to the next is hindered (Figure 1a). One reason for such compartmentalization is the cortical actin cytoskeleton, which usually forms a meshwork and might act as a barrier for diffusion. As a consequence of this hop or compartmentalized diffusion, apparent diffusion coefficients measured for large observation spots (D_{max}) are rather low since a molecular transits involve crossing of several of these barriers, while those measured for small observation spots (D_{max}) are large since they probe the free diffusion inside the compartments only.[13,25] This characteristic was reflected in our data, but present for a few points only. A recent study indicated that hop diffusion was not a dominant feature in STED-FCS recordings on PtK2 cells due to an average meshwork size of 25 nm, i.e., below the spatial resolution of those as well as our current measurements.[25] The few incidences of hop diffusion might indicate larger meshwork sizes at that point in space and time.

Our previous STED-FCS recordings demonstrated a dependency of the transient trapping of SM on levels of cholesterol and on the actin cytoskeleton.[13] Figure 3c,d depicts the scatter in value pairs (D_{max}, Δ_D) as determined from STED-FLCS recordings of SM diffusion in the plasma membrane of live Ptk2 cells treated with Latrunculin B (LatrB, for actin cytoskeleton depolymerization) or Cholesterol Oxidase (COase, for cholesterol depletion). While the overall variation in values of D_{max} and Δ_D was still strong, the extent of trapping decreased, as reflected by an overall increase in values of Δ_D (and more strongly for COase than for LatrB, compare also Figure S6). The STED-FLCS data confirmed our previous observations that the transient interactions of SM were cholesterol assisted and the mobility of the binding partners was hindered by the actin cytoskeleton.[13] Yet, our STED-FLCS data now allowed us to take a closer look on whether heterogeneity in membrane mobility had changed upon COase or LatrB treatments. Figure 3e,f depicts the boxplots (average and standard deviations) of the values D_{max} and Δ_D for all cases, diffusion of PE, of SM, and of SM following COase or LatrB treatments. For SM we have differentiated between events of strong trapping (D_{max}< 0.14) and weak trapping or free diffusion (D_{max} > 0.14). Clearly, as noted before, average values of both D_{max} and Δ_D were highest for the generally free diffusing PE lipid analogue, and those of SM whether for the case of D_0 > 0.14 or after LatrB or COase treatment all revealed weak trapping only. However, more notably, the standard deviations indicate that the variation in both overall macroscopic mobility (D_{max}) and more strongly in differences in diffusion modes (Δ_D) was reduced following COase treatment. Consequently, heterogeneity in lipid diffusion dynamics was reduced upon cholesterol depletion.

For the drug treatments, one cannot fully exclude incidences where a cell started apoptosis. However, we applied concentrations and incubation times for these drugs (Supporting Information) as used multiple times before in membrane diffusion studies, allowing a safe comparison.[5,12,13] In addition, we checked for a correlation between trapping Δ_D and fluorescent lipid analogue concentration. We estimated the concentration from the average particle number $N = 1/G(0)$ in the observation spot (calculated from the amplitude $G(0)$ of the correlation data generated for large observation spots) and determined a random distribution in value pairs (Δ_D, N) and no notable change in scatter of values when changing the concentration in fluorescent lipid analogues by an order of magnitude (Figure S8).

In conclusion, we have introduced STED-FLCS as an advanced tool to investigate molecular diffusion modes and especially their spatiotemporal dynamics. We highlighted changes in diffusion modes with a time resolution of down to a few seconds. Extending our previous studies, we now demonstrated large spatiotemporal heterogeneity in the diffusion dynamics of fluorescent lipid analogues in the plasma membrane of living cells. Specifically, a sphingolipid analogue SM showed distinct temporal and spatial incidences of interaction or trapping sites, where, as pointed out before,[12,13,27] individual lipids resided for approximately 10 ms. The interaction sites were transient for at least a few seconds, and confirmed previous scanning FCS data, but now directly highlighting that the diffusion mode in these trapping sites was indeed transient trapping. As expected, treatments for cholesterol depletion and actin depolymerization reduced the occurrence of these interaction sites. However, STED-FLCS

DOI: 10.1021/acs.nanolett.5b02001
Nano Lett. 2015, 15, 5912−5918

also for the first time demonstrated a slight reduction in the spatiotemporal heterogeneity of lipid diffusion upon treatment for cholesterol depletion, specifically with regards to changes in diffusion mode. We have to note that due to the need to record data for at least 10 s (to reach an accurate enough signal-to-noise ratio) the STED-FLCS recordings averaged over any heterogeneity on faster time scales than around a second. The only way to increase the time resolution will be the development of fluorescent labels with further increased brightness. An option in STED-FLCS analysis is the adaptation of the width ΔT of the gating window to the position of the time gate T_g, specifically reducing the width for smaller T_g and thus optimizing the range of accessible observation spot diameters from a single recording (Figure S5d), as discussed above. In addition, STED-FLCS can readily be applied on a commercial STED setup (Figure S9). The ultimate STED-FCS measurement would be scanning STED-FLCS, i.e., the combination of fast beam-scanning and STED-FLCS, allowing the simultaneous disclosure of diffusion modes ($D(d)$ dependencies) at different spatial points (e.g., along a line or circle). This would with great precision allow highlighting changes in heterogeneity of lipid diffusion dynamics over different parts of a single cell (e.g., cell body versus lamellipodia). STED-FLCS represents a new technology to highlight important molecular processes in the cellular plasma membrane, but should be extendable to other (intracellular) membranes or cytosolic processes.

■ ASSOCIATED CONTENT

Supporting Information

The Supporting Information is available free of charge on the ACS Publications website at DOI: 10.1021/acs.nanolett.5b02001.

Additional figures, materials, methods, and theory (PDF)

■ AUTHOR INFORMATION

Corresponding Authors

*E-mail: giuseppe.vicidomini@iit.it.

*E-mail: christian.eggeling@rdm.ox.ac.uk.

Author Contributions

The manuscript was written through contributions of all authors. All authors have given approval to the final version of the manuscript. G.V., H.T., V.M., and A.H. performed experiments, G.V. and C.E. analyzed data, M.B.C. and D.W. recorded and analyzed the data on the commercial system, E.S. and S.G. recorded data on SM in SLBs for the revised version of the manuscript, G.V., C.E., A.H., A.D., and S.W.H. conceived and designed research. G.V. and C.E. wrote the manuscript with feedback from all other authors.

Notes

The authors declare no competing financial interest.

■ ACKNOWLEDGMENTS

We would like to acknowledge numerous fruitful discussions and advices from Andreas Schönle, Gael Moneron and Kyu Young Han, and Tanja Gilat and Ellen Rothermel (MPI-BPC Göttingen) for helpful assistance. This work was supported in part by the PRIN No. 2008S22MJC 005 grant to A.D. and G.V, by the German Research Foundation within the SFB 755 (project B11) to C.E. and S.W.H., by the MRC, BBSRC, ESPRC, the Wolfson Foundation and the Wellcome Trust to C.E., D.W., and S.G., by a Marie-Curie fellowship to E.S., and by an Alfred Benzon Foundation research stipend to M.P.C.

■ ABBREVIATIONS

STED, stimulate emission depletion; FCS, fluorescence correlation spectroscopy; FLCS, fluorescence lifetime correlation spectroscopy; gSTED, gated STED; PE, phosphoethanolamine; SM, sphingomyelin; COase, cholesterol oxidase; LatrB, Latrunculin B; CW, continuous-wave; TCSPC, time-correlated single-photon counting

■ REFERENCES

(1) Lingwood, D.; Simons, K. *Science* **2010**, *327*, 46−50.

(2) Gowrishankar, K.; Ghosh, S.; Saha, S.; C, R.; Mayor, M.; Rao, M. *Cell* **2012**, *149*, 1353−1367.

(3) Kraft, M. L. *Mol. Biol. Cell* **2013**, *24*, 2765−2768.

(4) Kusumi, A.; Nakada, C.; Ritchie, K.; Murase, K.; Suzuki, K.; Murakoshi, H.; Kasai, R. S.; Kondo, J.; Fujiwara, T. *Annu. Rev. Biophys. Biomol. Struct.* **2005**, *34*, 351−378.

(5) Lenne, P. F.; Wawrezinieck, L.; Conchonaud, F.; Wurtz, O.; Boned, A.; Guo, X. J.; Rigneault, H.; He, H. T.; Marguet, D. *EMBO J.* **2006**, *25*, 3245−3256.

(6) Magde, D.; Webb, W. W.; Elson, E. *Phys. Rev. Lett.* **1972**, *29*, 705−708.

(7) Ehrenberg, M.; Rigler, R. *Chem. Phys.* **1974**, *4*, 390−401.

(8) Schwille, P.; Korlach, J.; Webb, W. W. *Cytometry* **1999**, *36*, 176−182.

(9) Ruan, Q. Q.; Cheng, M. A.; Levi, M.; Gratton, E.; Mantulin, W. W. *Biophys. J.* **2004**, *87*, 1260−1267.

(10) Wawrezinieck, L.; Rigneault, H.; Marguet, D.; Lenne, P. F. *Biophys. J.* **2005**, *89*, 4029−4042.

(11) Kastrup, L.; Blom, H.; Eggeling, C.; Hell, S. W. *Phys. Rev. Lett.* **2005**, *94*, 178104.

(12) Eggeling, C.; Ringemann, C.; Medda, R.; Schwarzmann, G.; Sandhoff, K.; Polyakova, S.; Belov, V. N.; Hein, B.; von Middendorff, C.; Schonle, A.; Hell, S. W. *Nature* **2009**, *457*, 1159−1162.

(13) Mueller, V.; Ringemann, C.; Honigmann, A.; Schwarzmann, G.; Medda, R.; Leutenegger, M.; Polyakova, S.; Belov, V. N.; Hell, S. W.; Eggeling, C. *Biophys. J.* **2011**, *101*, 1651−1660.

(14) Honigmann, A.; Mueller, V.; Ta, H.; Schoenle, A.; Sezgin, E.; Hell, S. W.; Eggeling, C. *Nat. Commun.* **2014**, *5*, 5412.

(15) Mueller, V.; Honigmann, A.; Ringemann, C.; Medda, R.; Schwarzmann, G.; Eggeling, C. FCS in STED Microscopy: Studying the Nanoscale of Lipid Membrane Dynamics. In *Methods in Enzymology*, Tetin, S. Y., Ed.; Elsevier Academic Press: Burlington, 2013; Vol. *591*, pp 1−38.

(16) Honigmann, A.; Mueller, V.; Hell, S. W.; Eggeling, C. *Faraday Discuss.* **2013**, *161*, 77−89.

(17) Moffitt, J. R.; Osseforth, C.; Michaelis, J. *Opt. Express* **2011**, *19*, 4242−4254.

(18) Vicidomini, G.; Moneron, G.; Han, K. Y.; Westphal, V.; Ta, H.; Reuss, M.; Engelhardt, H.; Eggeling, C.; Hell, S. W. *Nat. Methods* **2011**, *8*, 571−573.

(19) Vicidomini, G.; Schoenle, A.; Ta, H.; Han, K. Y.; Moneron, G.; Eggeling, C.; Hell, S. W. *PLoS One* **2013**, *8*, e54421.

(20) Lamb, D. C.; Schenk, A.; Rocker, C.; Scalfi-Happ, C.; Nienhaus, G. U. *Biophys. J.* **2000**, *79*, 1129−1138.

(21) Bohmer, M.; Wahl, M.; Rahn, H. J.; Erdmann, R.; Enderlein, J. *Chem. Phys. Lett.* **2002**, *353*, 439−445.

(22) Leutenegger, M.; Eggeling, C.; Hell, S. W. *Opt. Express* **2010**, *18*, 26417.

(23) Marrocco, M. *Chem. Phys. Lett.* **2007**, *449*, 227−230.

(24) Blom, H.; Björk, G. *Appl. Opt.* **2010**, *48*, 6050−6058.

(25) Andrade, D. M.; Clausen, M. P.; Keller, J.; Mueller, V.; Göttfert, F.; Bear, J. E.; Hell, S. W.; Lagerholm, B. C.; Eggeling, C. *Sci. Rep.* **2015**, *5*, 11454.

(26) Fujiwara, T.; Ritchie, K.; Murakoshi, H.; Jacobson, K.; Kusumi, A. *J. Cell Biol.* **2002**, *157*, 1071−1081.

DOI: 10.1021/acs.nanolett.5b02001
Nano Lett. 2015, 15, 5912−5918

(27) Ringemann, C.; Harke, B.; von Middendorff, C.; Medda, R.; Honigmann, A.; Wagner, R.; Leutenegger, M.; Schoenle, A.; Hell, S.; Eggeling, C. *New J. Phys.* **2009**, *11*, 103054.

DOI: 10.1021/acs.nanolett.5b02001
Nano Lett. 2015, 15, 5912−5918